Electronic Supplementary Information

Title: Dynamic reversible bonds enable external stress-free two-way shape memory effect of polymer network and the interrelated intrinsic self-healability of wider crack and recyclability

Authors: Long Fei Fan, Min Zhi Rong*, Ming Qiu Zhang* and Xu Dong Chen*

Evaluation of self-healing performance of the materials was conducted by two groups of experiments as follows.

(i) For verification of the intrinsic self-healing ability, the dumbbell-shaped PU specimen (total length = 50 mm, length of reduced section = 20 mm, width = 4 mm, and thickness = 1 mm) was bisected, and then the broken parts were manually recombined to keep the faces of the two halves in alignment and intimate contact. Healing proceeded at 100 °C for different times. Afterwards, the healed specimen was measured by tensile tests at 25 °C according to ISO527-2 using a universal tester (CMT 6000, SANS, China) at a crosshead speed of 50 mm/min. The strength ratio of the healed specimen to the virgin specimen gives the measure of healing efficiency:

$$\text{Healing efficiency} = \frac{\sigma_{healed}}{\sigma_{virgin}} \tag{S1}$$

where σ_{virgin} and σ_{healed} denote tensile strengths of virgin and healed specimen.

Because tensile strength of the virgin specimen cannot be fully restored, the reconnected interface became the weakest part, and had to break again during the subsequent tensile tests. This ensured that the second and third tensile failures happened to the same healed portion. That is, for quantifying efficiency of the second and third healing, the healed specimen was no longer cut like the virgin one, but subjected to repeated tensile tests and healing treatments. Healing efficiencies of multiple healing were thus calculated.

(ii) For examination of the self-healing assisted by shape memory effect, three virgin specimens were used. The first one was directly tested to failure under tension, offering the tensile strength, σ_{virgin}. The second one was half-cut to produce a wider crack (~250 μm wide, ~0.5 mm deep, which is half the thickness of the specimen) in the middle and along the thickness direction of the dumbbell-shaped specimen, and tested to failure under tension, offering tensile strength, $\sigma_{half-cut}$. The third one was half-cut, healed with the help of shape memory effect, and finally tested to failure under tension, offering tensile strength, σ_{healed}. In this case, healing efficiency is defined as:

$$\text{Healing efficiency} = \frac{\sigma_{healed} - \sigma_{half-cut}}{\sigma_{virgin} - \sigma_{half-cut}} \tag{S2}$$

To examine the reproducibility of the healability, a new specimen was half-cut, healed, reprogrammed, half-cut again on the healed place, healed for the second time, and eventually measured by tensile test. Furthermore, another new specimen was repeatedly half-cut and healed on the same place for three times and then subjected to tensile test. Accordingly, the multiple healability was characterized. To ensure the reproducibility of making wider crack on the same place of the specimen, a fixture that fixed the specimen and controlled the blade for cutting was employed.

Tab. S1 One-way SMPs using reversible bonds as the reversible segments

| Polymers	Reversible bonds	Ref.
Poly(*n*-butyl acrylate)	Hydrogen bond	S1
Copolymer of butyl acrylate (BA), trimethylolpropane trimethacrylate (TMP-TMA) and ureidopyrimidinone-substituted ethyl methacrylate (UPy-EMA)	Hydrogen bond	S2
Copolymer of 4-methacryloyloxy benzophenone, UPy-EMA and BA	Hydrogen bond	S3
Thermoplastic polyurethane (PU) with quadruple hydrogen bonding	Hydrogen bond	S4
(Meth) acrylate copolymers	Hydrogen bond	S5
PU	Hydrogen bond	S6
PU	Hydrogen bond	S7
PU	Hydrogen bond	S8
Poly(methacrylic acid-*co*-methy methacrylate)/poly(ethylene glycol) complexes	Hydrogen bond	S9
Poly(acrylic acid-*co*-methacrylate)/poly(ethylene glycol) complexes	Hydrogen bond	S10
Poly(methyl methacrylate)-*co*-(N-vinyl-2-pyrrolidone)/poly(ethylene glycol) semi-interpenetrating polymer	Hydrogen bond	S11
poly(methyl acrylate)-*co*-(acrylic acid)	Hydrogen bond	S12
poly(ethylene glycol)-UPy copolymer	Hydrogen bond	S13
Polyacrylamide-based hydrogel	Hydrogen bond	S14
Polylactide/hydroxyapatite nanocomposites	Hydrogen bond	S15
Cellulose-whiskers/PU nanocomposites	Hydrogen bond	S16
Graphene-poly(acrylamide-*co*-acrylic acid) hybrid materials	Hydrogen bond	S17
Polyvinyl alcohol/graphene oxide nanocomposites	Hydrogen bond	S18
PU/cotton cellulose nanowhiskers nanocomposites	Hydrogen bond	S19
Polylefin elastomer/modified graphene nanocomposites	Hydrogen bond	S20
Poly(glycerol sebacate)	Hydrogen bond	S21
Polyvinylpyrrolidone/ poly(hydroxyethyl methacrylate-*co*-butyl acrylate) semi-IPNs	Hydrogen bond	S22
Epoxidized natural rubber	Hydrogen bond	S23
PU ionomer	Ionic interactions	S24
Poly(ether ether ketone) (PEEK)	Ionic interactions	S25
Sulfonated PEEK ionomers	Ionic interactions	S26
Mixtures of elastomeric ionomer and fatty acids or their salts	Ionic interactions	S27
Copolymer of acrylamide and acrylic acid with low amounts of a cationic surfmer	Ionic interactions	S28
Cellulose-butyl-3-methylimidazolium chloride gel	Ionic interactions	S29
Supramolecular hydrogels composed of phenylboronic acid modified sodium alginate and poly(vinyl alcohol)	Ionic interactions	S30
Polybutadiene	Ionic interactions	S31
Copolymer of *n*-Octadecyl acrylate, acrylamdie and arcylic acid	Ionic interactions	S32
Poly(acrylic acid)-graphene oxide-Fe^{3+} hydrogel	Ionic interactions	S33
Polybutadiene	Metal-ligand coordination	S34
Poly(*p*-dioxanone) metallosupramolecular network	Metal-ligand coordination	S35
Copolymer of stearyl methacrylate, acrylamide, and acrylic acid	Metal-ligand coordination	S36
Polyimides	π-π stacking	S37
Pentaerythritol tetra(3-mercaptopropionate)2-methylene-propane-1,3-di(thioethyl vinyl ether)	Allyl sulfide	S38
Epoxy networks	Hydroxy-ester	S39
Sodium alginate	Phenylboronic acid-catechol interactions	S40
Copolymer of *N,N*-dimethylacrylamide, 2-hydroxyethyl acrylate and boric acid	Boronate ester	S41
Copolymer of *n*-butylacrylate, hydroxyethyl methacrylate and ethyleneglycol-1-acrylate-2-cinnamic acid	Cinnamic groups	S42
PU	Diels-Alder bond	S43
Polyesterurethane	Diels-Alder bond	S44
Poly(styrene-*block*-butadiene-*block*-styrene)	Diels-Alder bond	S45
Epoxy	Diels-Alder bond	S46
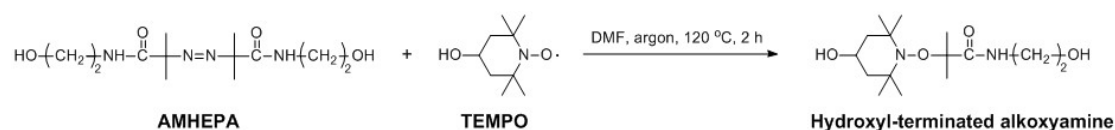
Fig. S1 Synthesis of hydroxyl-terminated alkoxyamine.
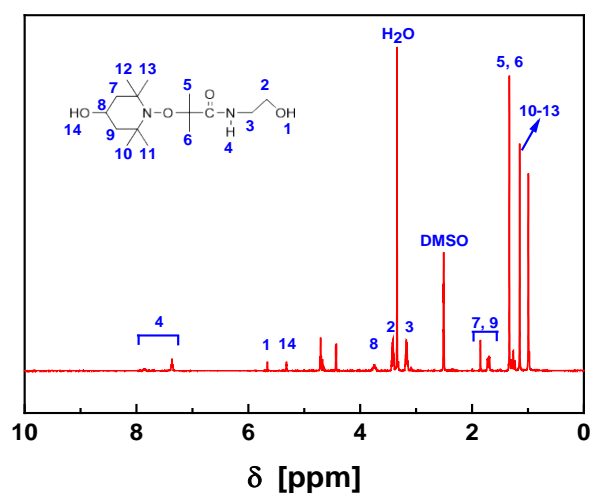
Fig. S2 ^{1}H NMR spectrum of hydroxyl-terminated alkoxyamine.
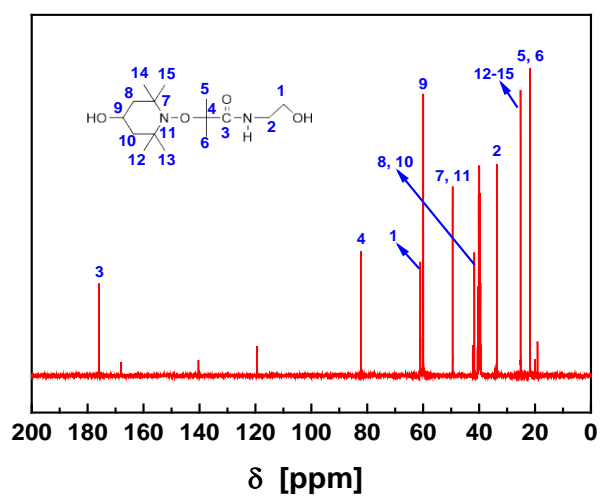

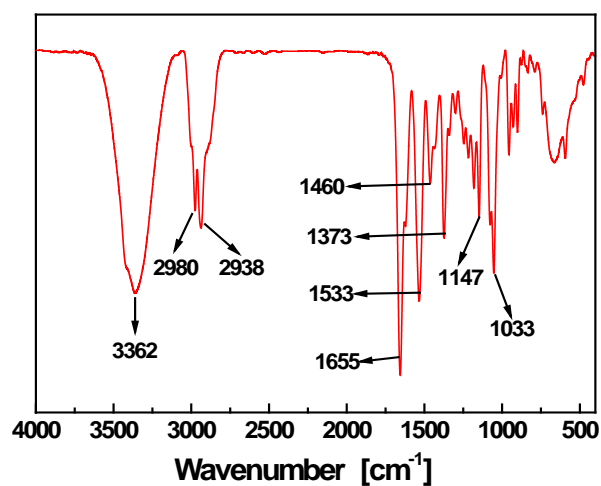**Fig. S3** ^{13}C NMR spectrum of hydroxyl-terminated alkoxyamine.

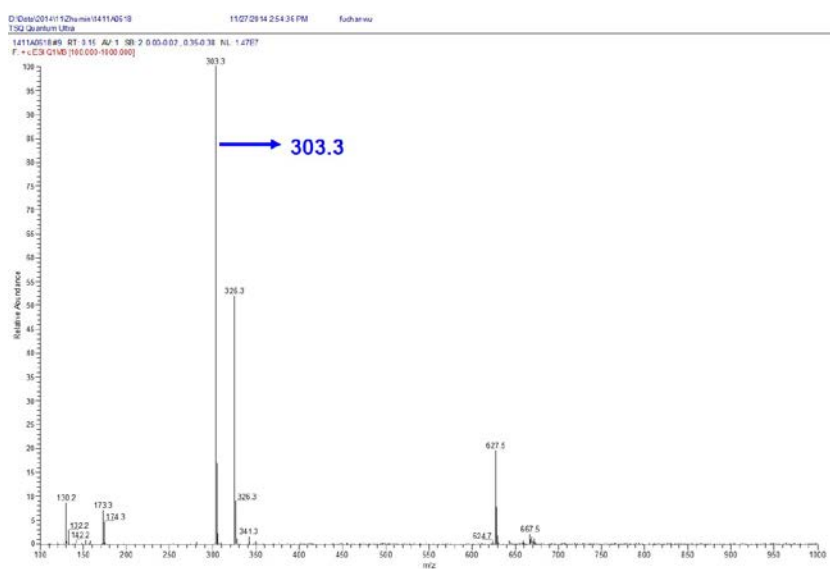**Fig. S4** FTIR spectrum of hydroxyl-terminated alkoxyamine.

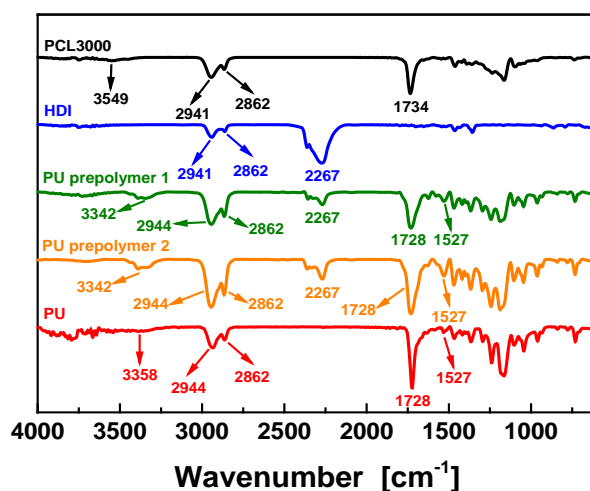**Fig. S5** Mass spectrum of hydroxyl-terminated alkoxyamine.

Fig. S6 FTIR spectra of HDI, PCL, PU prepolymer 1, PU prepolymer 2 and PU. FTIR (KBr/cm^{-1}): PCL (3549, 2941, 2862, 1734, and 1462), HDI (2941, 2862, 2267, and 1464), PU prepolymer 1 (3342, 2944, 2862, 2267, 1728, 1527, and 1467), PU prepolymer 2 (3342, 2944, 2862, 2267, 1728, 1527, and 1467), and PU (3348, 2944, 2862, 1728, 1527, and 1466).
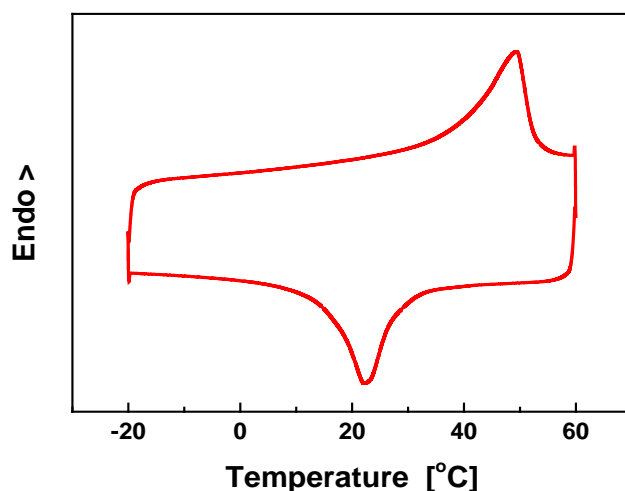
Fig. S7 DSC heating and cooling scans of the crosslinked PU (ramp: 3 °C/min). The crystallinity (X_c) calculated from $\Delta H_f / \Delta H_f°$ (where ΔH_f denotes the measured heat of fusion, and $\Delta H_f°$ is the heat of fusion of 100% crystalline PCL (139.5 J g^{-1} [S47])) is found to be 24.3%.
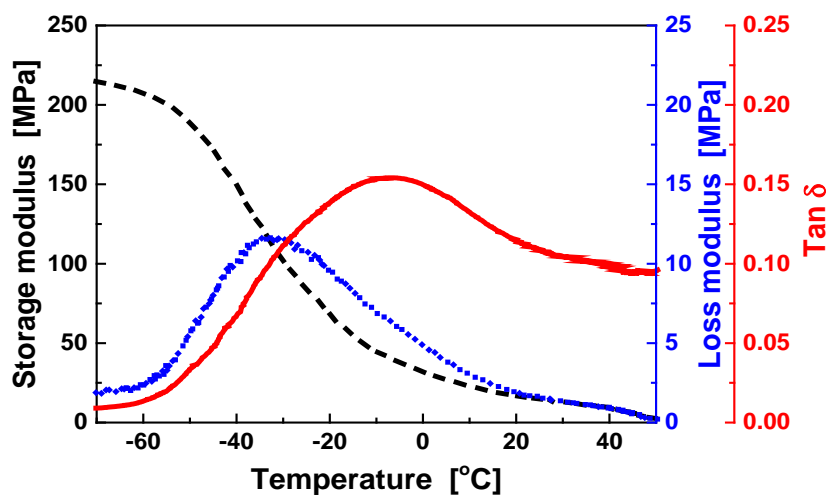
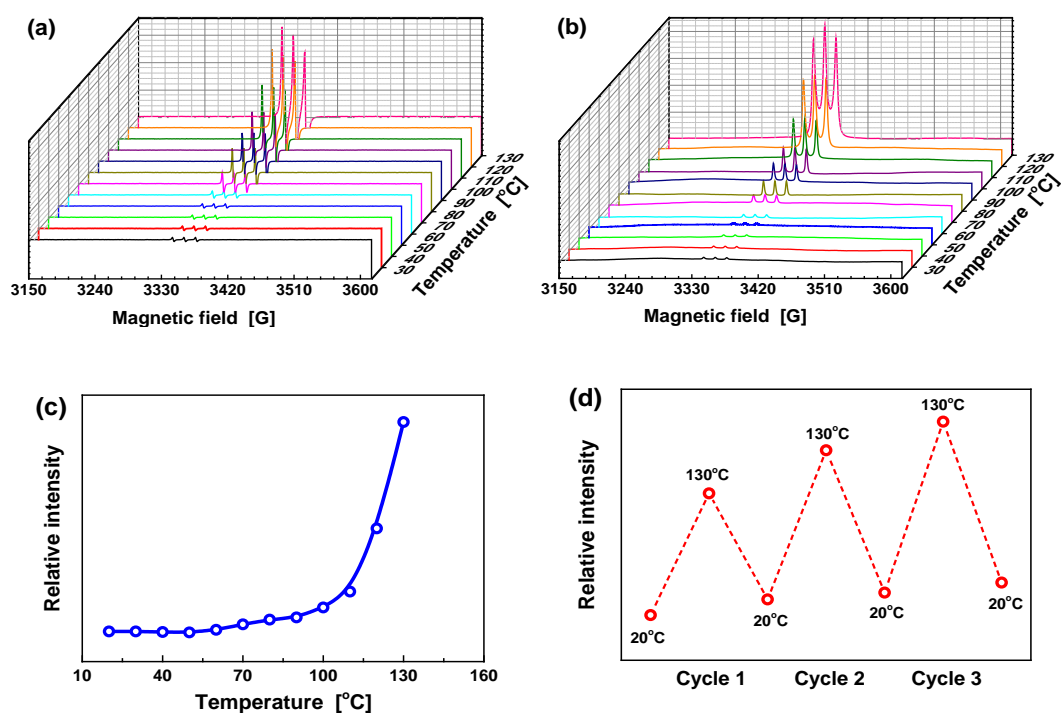**Fig. S8** DMA spectra of the crosslinked PU (ramp: 3 °C/min; frequency: 1 Hz).

Fig. S9 (a) Typical ESR spectra of hydroxyl-terminated alkoxyamine measured at various temperatures. (b) Normalized absorption lines converted from the data of (a). (c) Temperature dependence of relative ESR signal intensities calculated from integral areas of the normalized absorption curves in (b). (d) Relative ESR signal intensities measured during heating-cooling cycles between 20 and 130 °C.
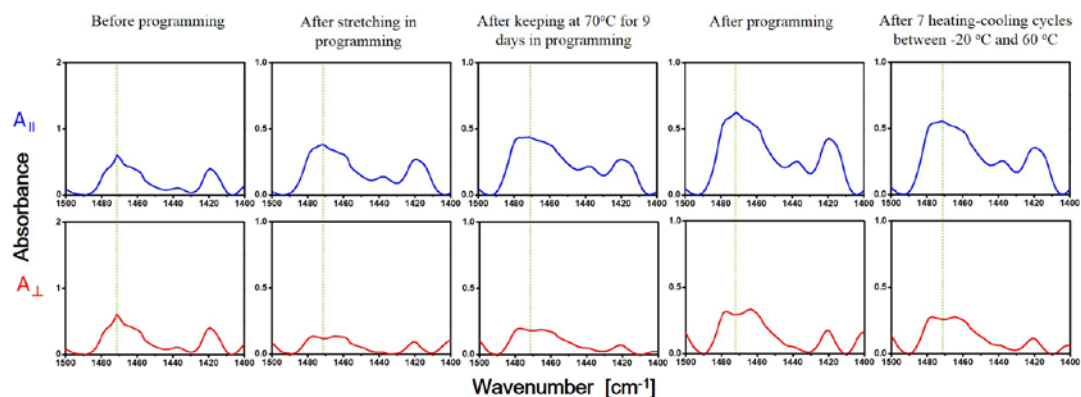
Fig. S10 δ(-CH$_2$-) region on the FTIR spectra of the crosslinked PU specimens. Note: The specimen measured after stretching in programming means that it was deformed to a temporary shape with strain of 1000 % (refer to step ② in **Fig. 6**) and cooled down to room temperature for the FTIR measurement. The specimen measured after keeping at 70 °C for 9 days in programming refers to that obtained after step ⑤ in **Fig. 6**.

Tab. S2 Characterization of orientation of the crosslinked PU specimen based on the measurement of FTIR dichroism in **Fig. S10**

| Sample	Before programming	After stretching in programming	After keeping at 70°C for 9 days in programming	After programming	After 7 heating-cooling cycles between RT and 60°C
A$_{//}$	0.6	0.38	0.44	0.63	0.56
A$_{\perp}$	0.6	0.12	0.18	0.29	0.26
R	1	3.17	2.44	2.17	2.15
(R-1)/(R+2)	0	0.42	0.32	0.28	0.28
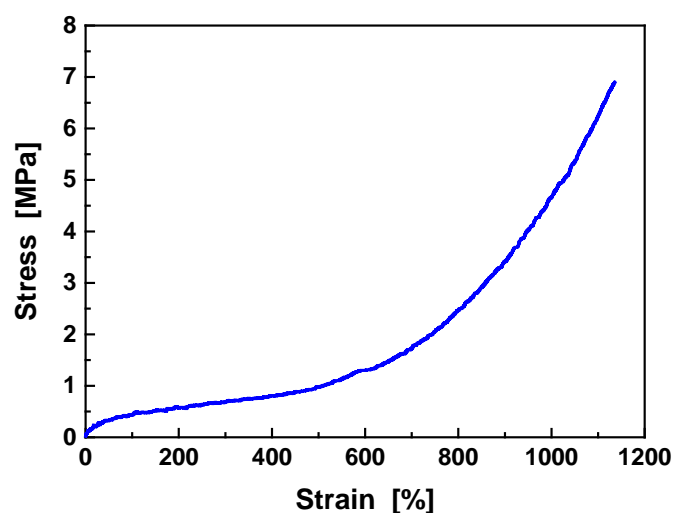
Fig. S11 Typical tensile stress-strain curve of the crosslinked PU measured at 60 °C. Prior to the test, the specimen was firstly immersed in the THF solution of LiBr (500 mL, 20 g/L) for 24 h at room temperature to remove the inter- and intra-macromolecular hydrogen bonds [S48-S50]. Then, the specimen was dried at room temperature for 24 h allowing for evaporation of THF. Finally, the specimen was heated to 60 °C for 2 min and tested to failure under tension.
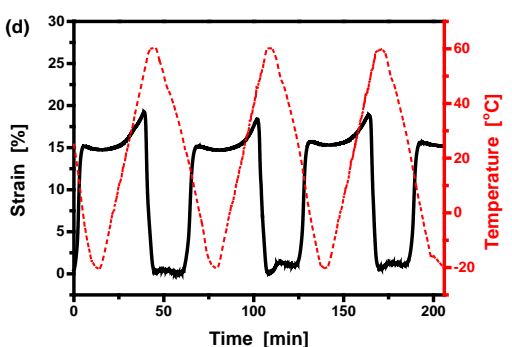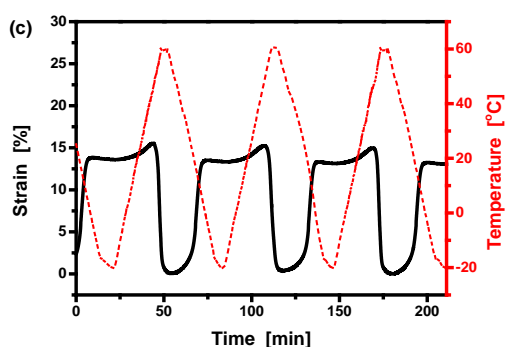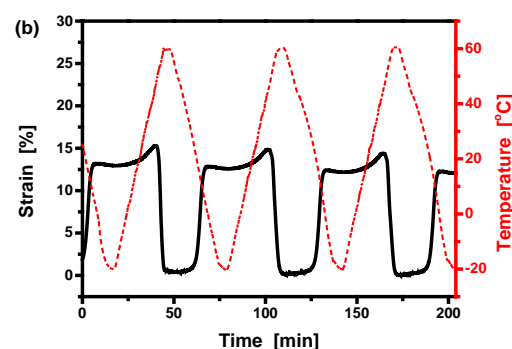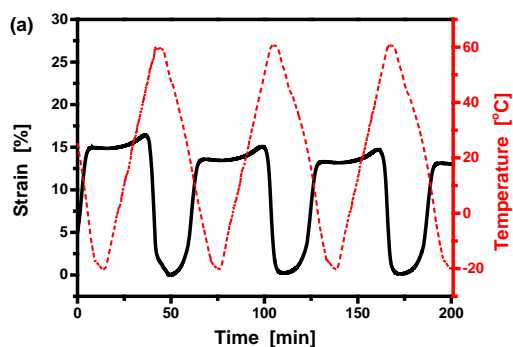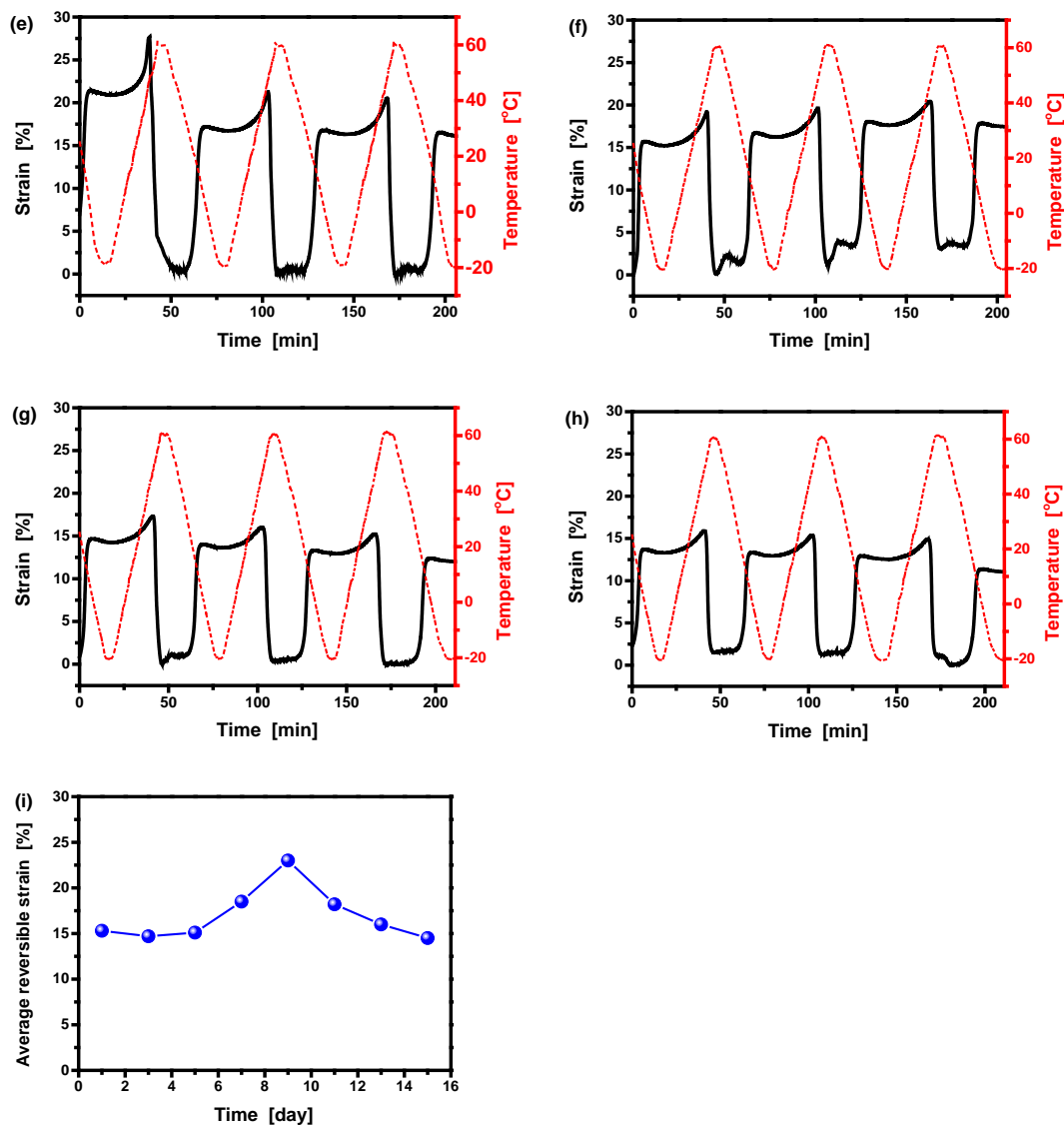
Fig. S12 (a)-(h) Reversible strain measured by DMA of the programmed PU during repeated heating and cooling cycles between -20 and 60 °C (ramp: 3 °C/min). Training times: (a) 1 day, (b) 3 days, (c) 5 days, (d) 7 days, (e) 9 days, (f) 11 days, (g) 13 days, and (h) 15 days. (i) Average reversible strains of the specimens versus training time.
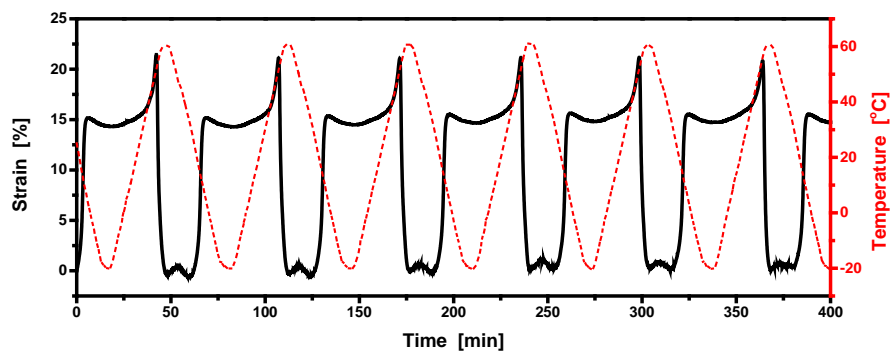
Fig. S13 Thermomechanical behavior (measured by DMA) of the reprogrammed crosslinked PU during repeated heating and cooling cycles between -20 and 60 °C (ramp: 3 °C/min).
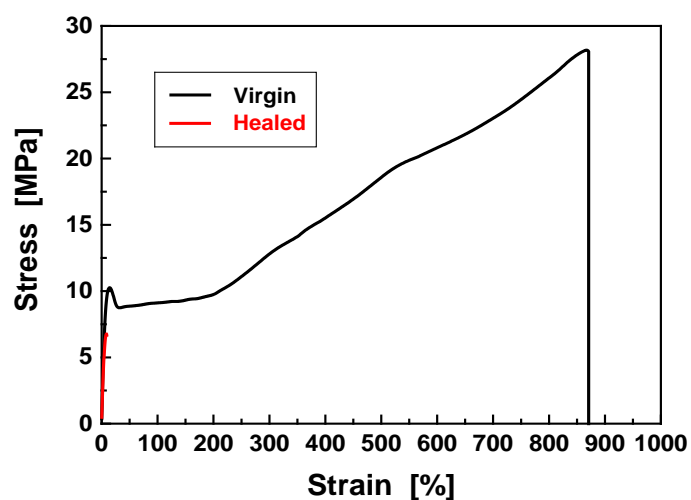

Fig. S14 Typical tensile stress-strain curves of virgin and healed control specimens. The control sample was synthesized following the same procedures applied to the production of the crosslinked PU, while hydroxyl-terminated alkoxyamine was replaced by 1,4-butanediol (BDO). Then, the dumbbell-shaped specimen of the control was bisected, manually recombined, healed at 100 ºC for 24 h, and measured by tensile test.
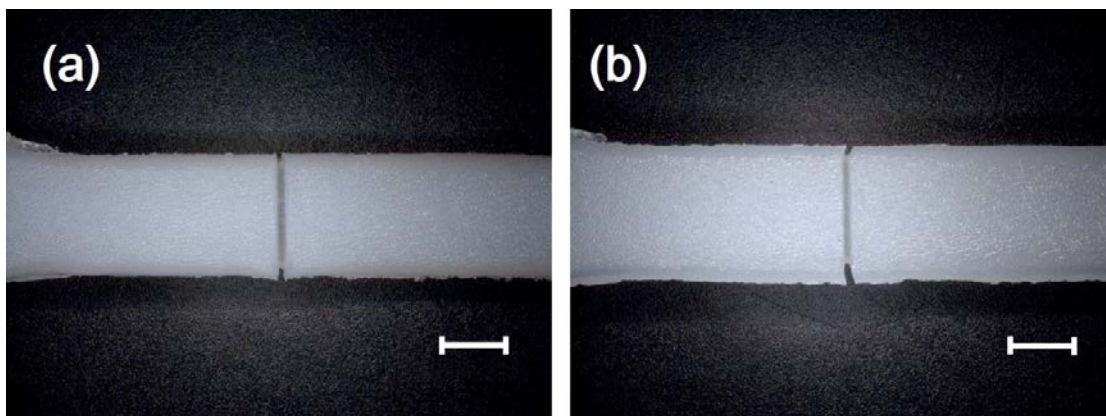
Fig. S15 Photos showing the half-cut crack on the unprogrammed crosslinked PU specimen (a) before and (b) after healing at 100 ℃ for 24 h. The scale bar represents 2 mm in length.
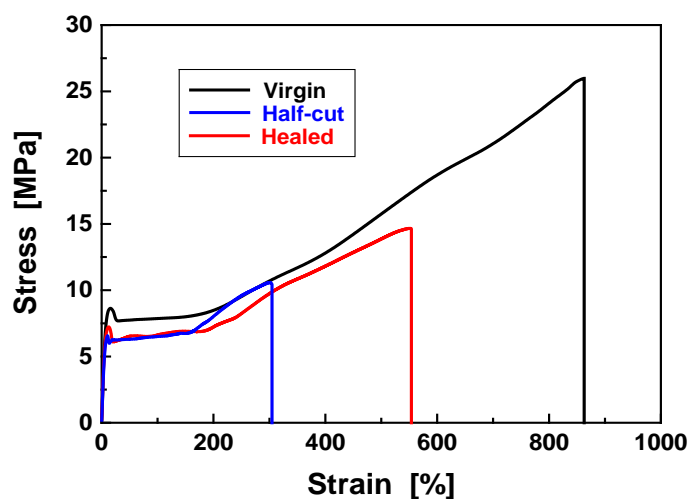

Fig. S16 Typical tensile stress-strain curves of virgin, half-cut and healed unprogrammed crosslinked PU specimens. Healing conditions: 100 ℃, 24 h.
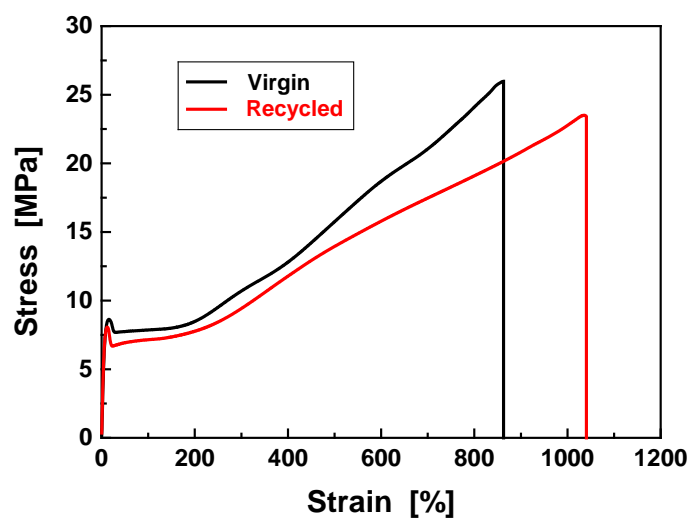

Fig. S17 Typical tensile stress-strain curves of the crosslinked PU and its recycled version.
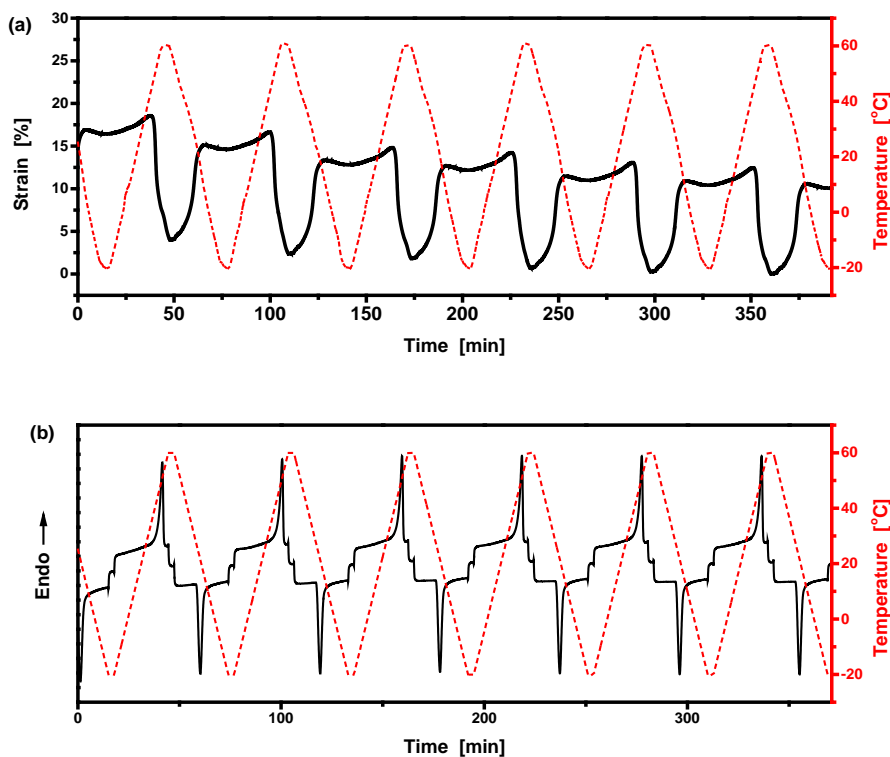
Fig. S18 (a) Thermomechanical behavior (measured by DMA) and (b) thermogram (measured by DSC) of the programmed recycled PU during repeated heating and cooling cycles between -20 and 60 °C (ramp: 3 °C/min). The first cycle that was used to remove the thermal history is not displayed for clarity.

Fig. S19 Typical tensile stress-strain curves of repeatedly healed recycled PU with the assistance of shape memory effect (crack size: ~250 μm wide and ~0.5 mm deep).

Supporting references

[S1] C. L. Lewis, K. Stewart and M. Anthamatten, *Macromolecules*, 2014, **47**, 729-740.

[S2] J. Li, J. A. Viveros, M. H. Wrue and M. Anthamatten, *Adv. Mater.*, 2007, **19**, 2851-2855.
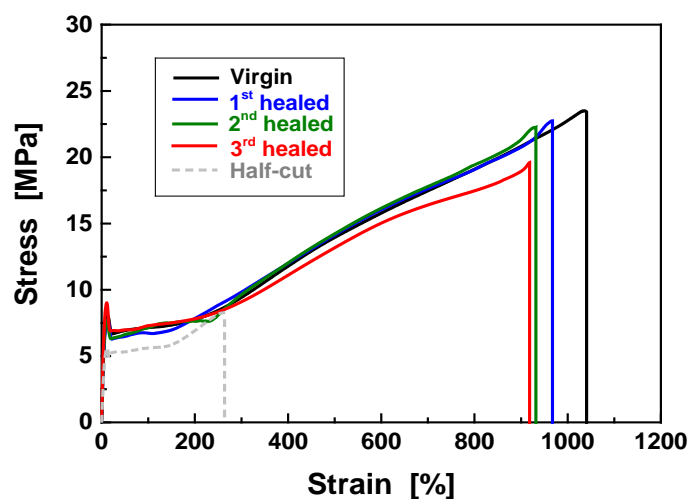
[S3] J. Li, C. L. Lewis, D. L. Chen and M. Anthamatten, *Macromolecules*, 2011, **44**, 5336-5343.

[S4] Y. Zhu, J. Hu and Y. Liu, *Eur. Phys. J. E*, 2009, **28**, 3-10.

[S5] T. Ware, K. Hearon, A. Lonnecker, K. L. Wooley, D. J. Maitland and W. Voit, *Macromolecules*, 2012, **45**, 1062-1069.

[S6] S. Chen, J. Hu, C. Yuen and L. Chan, *Polymer*, 2009, **50**, 4424-4428.

[S7] S. Chen, J. Hu, H. Zhou, C. Yuen and L. Chan, *Polymer*, 2010, **51**, 240-248.

[S8] S. Chen, J. Hu, H. Zhuo and S. Chen, *J. Mater. Sci.*, 2011, **46**, 5294-5304.

[S9] Y. Cao, Y. Guan, J. Du, Y. Peng, C. W. Yip and A. S. C. Chan, *Chinese J. Polym. Sci.*, 2003, **21**, 29-3.

[S10] G. Liu, X. Ding, Y. Cao, Z. Zheng and Y. Peng, *Macromolecules*, 2004, **37**, 2228-2232.

[S11] G. Liu, C. Guan, H. Xia, F. Guo, X. Ding and Y. Peng, *Macromol. Rapid Commun.*, 2006, **27**, 1100-1104.

[S12] Y. Pan, T. Liu, J. Li, Z. Zheng, X. Ding and Y. Peng, *J. Polym. Sci. Part B: Polym. Phys.*, 2011, **49**, 1241-1245.

[S13] M. Guo, L. M. Pitet, H. M. Wyss, M. Vos, P. Y. W. Dankers, E. W. Meijer, *J. Am. Chem. Soc.*, 2014, **136**, 6969-6977.

[S14] T. Zhao, M. Tan, Y. Cui, C. Deng, H. Huang and M. Guo, *Polym. Chem.*, 2014, **5**, 4965-4973.

[S15] S. Zhou, X. Zheng, X. Yu, J. Wang, J. Weng, X. Li, B. Feng and M. Yin, *Chem. Mater.*, 2007, **19**, 247-253.

[S16] H. Luo, J. Hu and Y. Zhu, *Macromol. Chem. Phys.*, 2011, **212**, 1981-1986.

[S17] J. Dong, J. Ding, J. Weng and L. Dai, *Macromol. Rapid Commun.*, 2013, **34**, 659-664.

[S18] X. Qi, X. Yao, S. Deng, T. Zhou and Q. Fu, *J. Mater. Chem. A*, 2014, **2**, 2240-2249.

[S19] J. Mendez, P. K. Annamalai, S. J. Eichhorn, R. Rusli, S. J. Rowan, E. J. Foster and C. Weder, *Macromolecules*, 2011, **44**, 6827-6835.

[S20] M. Kashif and Y.-W Chang, *Eur. Polym. J.*, 2015, **66**, 273-281.

[S21] Y. Wu, L. Wang, X. Zhao, S. Hou, B. Guo and P. X. Ma, *Biomaterials*, 2016, **104**, 18-31.

[S22] Z.-C. Jiang, Y.-Y. Xiao, Y. Kang, B.-J. Li and S. Zhang, *Macromol. Rapid Commun.*, 2017, **38**, 1700149.

[S23] T. Lin, Z. Tang and B. Guo, *ACS Appl. Mater. Interfaces*, 2014, **6**, 21060-21068.

[S24] Y. Zhu, J. Hu, J. Lu, L. Y. Yeung and K. Yeung, *Polym. Adv. Technol.*, 2008, **19**, 1745-1753.

[S25] Y. Shi, M. Yoonessi and R. A. Weiss, *Macromolecules*, 2013, **46**, 4160-4167.

[S26] Y. Shi and R. A. Weiss, *Macromolecules*, 2014, **47**, 1732-1740.

[S27] R. A. Weiss, E. Izzo and S. Mandelbaum, *Macromolecules*, 2008, **41**, 2978-2980.

[S28] Y. Fan, W. Zhou, A. Yasin, H. Li and H. Yang, *Soft Matter*, 2015, **11**, 4218-4225.

[S29] H. Izawa, Y. Kaneko and J. Kadokawa, *J. Mater. Chem.*, 2009, **19**, 6969-6972.

[S30] H. Meng, P. Xiao, J. Gu, X. Wen, J. Xu, C. Zhao, J. Zhang and T. Chen, *Chem. Commun.*, 2014, **50**, 12277-12280.

[S31] D. Wang, J. Guo, H. Zhang, B. Cheng, H. Shen, N. Zhao and J. Xu, *J. Mater. Chem. A*, 2015, **3**, 12864-12872.

[S32] K. Peng, H. Yu, H. Yang, X. Hao, A. Yasin and X. Zhang, *Soft Matter*, 2017, **13**, 2135-2140.

[S33] L. Zhao, J. Huang, T. Wang, W. Sun and Z. Tong, *Macromol. Mater. Eng.*, 2017, **302**, 1600359.

[S34] J. R. Kumpfer and S. J. Rowan, *J. Am. Chem. Soc.*, 2011, **133**, 12866-12874.

[S35] T. Zhang, Z. Wen, Y. Hui, M. Yang, K. Yang, Q. Zhou and Y. Wang, *Polym. Chem.*, 2015, **6**, 4177-4184.

[S36] Z. Qin, R. Niu, C. Tang, J. Xia, F. Ji, D. Dong, H. Zhang, S. Zhang, J. Li and F. Yao, *Macromol. Mater. Eng.*, 2018, **303**, 1700396.

[S37] Q. Wang, Y. Bai, Y. Chen, J. Ju, F. Zheng and T. Wang, *J. Mater. Chem. A*, 2015, **3**, 352-359.

[S38] T. F. Scott, R. B. Draughon and C. N. Bowman, *Adv. Mater.*, 2006, **18**, 2128-2132.

[S39] D. Montarnal, M. Capelot, F. Tournilhac and L. Leibler, *Science*, 2011, **334**, 965-968.

[S40] Z. Li, W. Lu, T. Ngai, X. Le, J. Zheng, N. Zhao, Y. Huang, X. Wen, J. Zhang and T. Chen, *Polym. Chem.*, 2016, **7**, 5343-5346.

[S41] Y. Chen, W. Qian, R. Chen, H. Zhang, X. Li, D. Shi, W. Dong, M. Chen and Y. Zhao, *ACS Macro. Lett.*, 2017, **6**, 1129-1133.

[S42] A. Lendlein, H. Jiang, O. Jünger and R. Langer, *Nature*, 2005, **434**, 879-882.

[S43] X. Lu, G. Fei, H. Xia and Y. Zhao, *J. Mater. Chem. A*, 2014, **2**, 16051-16060.

[S44] J.-M. Raquez, S. Vanderstappen, F. Meyer, P. Verge, M. Alexandre, J.-M. Thomassin, C. Jerome and P. Dubois, *Chem. Eur. J.*, 2011, **17**, 10135-10143.

[S45] J. Bai and Z. Shi, *ACS Appl. Mater. Interfaces*, 2017, **9**, 27213-27222.

[S46] G. Zhang, Q. Zhao, L. Yang, W. Zou, X. Xi and T. Xie, *ACS Macro. Lett.*, 2016, **5**, 805-808.

[S47] V. Crescenzi, G. Manzini, G. Calzolari and C. Borri, *Eur. Polym. J.*, 1972, **8**, 449-463.

[S48] P. Alexander, *Ann. N. Y. Acad. Sci.*, 1951, **53**, 653-673.

[S49] K. I. Furuhata, K. Koganei, H. S. Chang, N. Aoki and M. Sakamoto, *Carbohydr. Res.*, 1992, **230**, 165-177.

[S50] H. Tseng, K. I. Furuhata and M. Sakamoto, *Carbohydr. Res.*, 1995, **270**, 149-161.